



HAL
open science

A novel approach for 3D morphological characterization of silica nanoparticle population through HAADF-STEM

Loïc Crouzier, Frédéric Pailloux, Alexandra Delvallée, Laurent Devoille,
Nicolas Feltin, Christophe Tromas

► To cite this version:

Loïc Crouzier, Frédéric Pailloux, Alexandra Delvallée, Laurent Devoille, Nicolas Feltin, et al.. A novel approach for 3D morphological characterization of silica nanoparticle population through HAADF-STEM. Measurement - Journal of the International Measurement Confederation (IMEKO), 2021, 180, pp.109521. 10.1016/j.measurement.2021.109521 . hal-04573699

HAL Id: hal-04573699

<https://hal.science/hal-04573699>

Submitted on 22 Jul 2024

HAL is a multi-disciplinary open access archive for the deposit and dissemination of scientific research documents, whether they are published or not. The documents may come from teaching and research institutions in France or abroad, or from public or private research centers.

L'archive ouverte pluridisciplinaire **HAL**, est destinée au dépôt et à la diffusion de documents scientifiques de niveau recherche, publiés ou non, émanant des établissements d'enseignement et de recherche français ou étrangers, des laboratoires publics ou privés.



Distributed under a Creative Commons Attribution - NonCommercial 4.0 International License

A novel approach for 3D morphological characterization of silica nanoparticle population through HAADF-STEM

Loïc Crouzier^{1,2}, Frédéric Pailloux², Alexandra Delvallée¹, Laurent Devoille¹, Nicolas Feltin¹, Christophe Tromas²

¹⁻ *Laboratoire National de métrologie et d'Essais - Nanometrology, 29 avenue Hennequin, 78197 Trappes Cedex (France)*

²⁻ *Institut Pprime Département Physique et Mécanique des Matériaux – 11 Bd Marie et Pierre Curie, 86962 Futuroscope Chasseneuil (France)*

Corresponding author: Loic.Crouzier@lne.fr

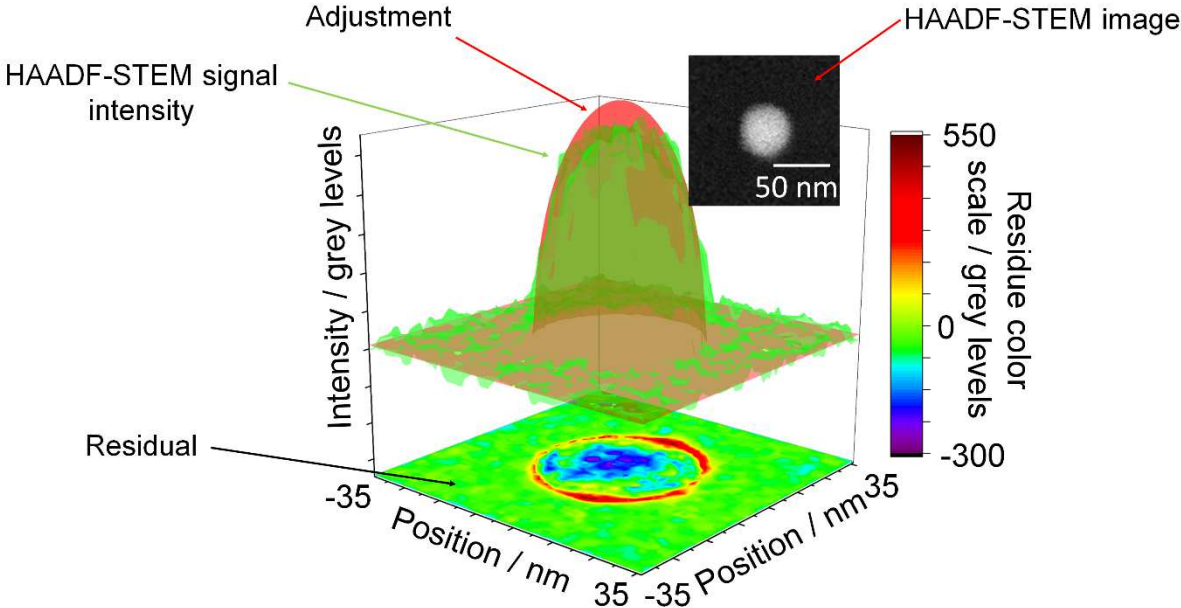
Keywords:

HAADF-STEM, Silica Nanoparticles, 3D Shape Measurement, Size Measurement, Metrology.

Abstract

The morphology of amorphous silica NPs in three dimensions (3D) of space is analysed using a single technique: the transmission electron microscope in Scanning Transmission Electron Microscopy with High Angle Annular Dark Field (HAADF-STEM) imaging mode. For this purpose, a method consisting in adjusting the HAADF-STEM signal by a function describing the thickness of material in a sphere has been developed to determine the height of the nano-object and tested on particles having quasi-spherical shape. This approach is suitable only in the case of a nanomaterial chemically homogeneous. A reference present in the image is required for calibrating the signal strength. This reference can be either a particle of known shape or a particle whose height was previously measured with another technique (*i.e.* Atomic Force Microscopy). Thus, the study of the small silica particles by HAADF-STEM highlighted their spheroidal shape but also their preferential orientation on the substrate.

Graphical abstract



1. Introduction

The physicochemical properties of a nanomaterial are directly related to its size and can be different from a material of the same chemical composition in its bulk state. Consequently, the interest and use of nanoparticles (NPs) by scientists and industrials has been constantly increasing. Thus, nowadays, it is common to find nanomaterials in food [1–3], cosmetics [4, 5], textile [6, 7], manufacturing [8] or even in health products [9, 10]. Regarding silica NP, because of their unique properties, they have attracted significant interest for medicine [11, 12], agricultural field [13, 14] or environmental bioremediation [15, 16]. Given the increasing use of nanomaterials, many regulations on the use of NPs have emerged in the last few years [17–20]. These regulations rely on an identification of the nanoparticles in a substance based on their dimensional properties (size, size distribution, shape, etc.) [21]. Therefore, industrial sector needs to characterise their products containing nanomaterials, *i.e.* to obtain information on the dimensional properties of NPs in the 3 dimensions of space.

Indirect measuring techniques such as Dynamic Light Scattering (DLS), Centrifugation Liquid Sedimentation (CLS) or single particle Inductively Coupled Plasma Mass Spectroscopy (sp-ICPMS) are limited for the study of non-spherical particles because their measurement is associated with an equivalent sphere [22–24]. Thus, several studies have focused on the use of direct techniques (microscopy) to characterise the dimensional properties of NPs population in 3D [25, 26]. There is no single low-cost technique for measuring these dimensions in 3D with controlled uncertainty. Thus, several solutions have been proposed such as the implementation of a hybrid approach combining two complementary techniques [25] or the acquisition by electron microscopy of images of the same particle with several angles of inclination to reconstruct its geometry [26]. Nevertheless, these methods are difficult to implement for large-scale analysis of nanoparticle populations.

However, for 3D quantitative analysis of NPs, electron microscopy in transmission can be used. Indeed, a recent study of Buhr *et al.* demonstrated the interest of a method linking the signal brightness to the thickness of the material probed during the analysis of silica particles by TSEM (Transmission Scanning Electron Microscopy) [27]. Because the signal depends on both density and thickness of the material passed through by electron beam (mass-thickness contrast), it is possible to obtain a quantitative measurement of nanoparticle height. In their study, the relationship between signal brightness and material thickness is established using Monte Carlo simulation of electron scattering. Thus, by using a single technique, the authors highlight a deviation from the sphericity of silica NPs below a certain size.

In our study, in order to reach the nanoparticle thickness we will use HAADF-STEM (Scanning Transmission Electron Microscopy with High Angle Annular Dark Field imaging mode). Compared to TSEM, this technique gives better resolution in the *XY* plane due to higher beam energies. Moreover, when studying homogeneous particles, the signal is related to the thickness of the material passed

through by the electron beam and linear up to a certain thickness depending on the nature of the imaged objects [28–30]. Here, an experimental approach was carried out by means of reference silica NPs whose sphericity is well known [25, 31] and enable to relate the signal intensity to the thickness of the material passed through. Thus, the aim of this study is to obtain a measure of the 3D dimensional properties of a NP from a single image. This will enable to overcome the shortcomings of similar characterization techniques requiring either a large quantity of images (electronic tomography) or the use of co-location tools for transfer between two techniques (hybrid metrology).

This method will make it possible to determine the nanoscale dimension of an object along the axis perpendicular to the substrate surface on which it is deposited. For instance, the thickness of a nanoplate population is typically impossible to be measured by electron microscopy-based techniques due to their natural orientation on the substrate. But these nano-objects with a single nanoscale dimension will be able to be fully characterized through this approach using a single microscopy technique, leading to time and money savings for industrials involved in nanomaterial field.

This study is divided as follows:

In a first step, the linearity of the STEM signal over the thickness range studied is checked on spherical reference particles. This is achieved by fitting the intensity profile along a particle with a function describing the thickness of a sphere.

In a second step, the dimensional parameter measurements by STEM are compared with Atomic Force Microscopy (AFM) and Scanning Electron Microscopy (SEM) measurements carried out on the same particles to validate this approach.

Finally, the use of reference for the calibration of the HAADF-STEM signal as a function of the thickness passed through by electron will make it possible to carry out a three-dimensional morphological characterization of silica NPs of more complex shape.

2. Materials and method

2.1. Samples

The silica NPs used in this study are certified reference nanomaterials (CRNM) provided by the European commission Join Research Center (JRC). Two different sizes of NPs were selected:

The ERM[®]-FD101b [31] NPs are provided as a stable silica colloidal suspension. This sample shows a bimodal particle size distribution with two well-separated particle populations (Figure 1): one around 40 nm and a second with certified diameter (number-weighted modal area equivalent diameter) equal to (83.7 ± 1.1) nm (coverage factor $k = 1$). In order to compare our measurements with the reference value, the certificate requires us to count and measure only particles with an equivalent diameter larger than 60 nm. The other mode (diameter close to 40 nm) was also studied but not as reference particles.

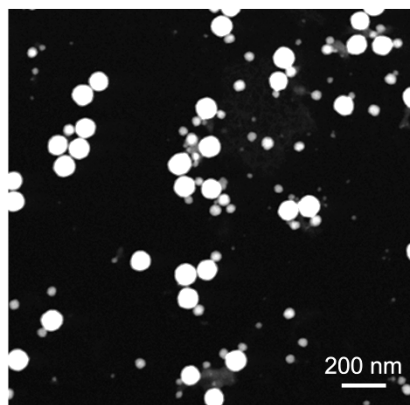


Figure 1 : HAADF-STEM image of ERM[®]-FD101b reference silica NPs.

The ERM[®]-FD304 [32] silica NPs sample consists also of a stable colloidal suspension. The number-weighted modal area equivalent diameter of ERM[®]-FD304 silica NPs is given as an indicative value for electron microscopy (SEM as well as TEM) and is equal to (27.8 ± 0.8) nm ($k = 1$).

2.2. Sample preparation

The “spin-coating” deposition method develop in ref. [33] and adapted in ref. [34] was used here to deposit NPs on microscopy grids (Agar Scientific AGS 160). The grid was functionalized with a layer of Poly-L-Lysine (PLL) prior to the NPs deposition to promote their adhesion. A specific set-up was installed to maintain the grid during “spin-coating” (Figure 2). A paraffin film (Parafilm[®] M) was used to fix the grid on a silicon substrate. The substrate was then placed on the vacuum system to be held in place during spin-coating step. Then a droplet of NP suspension was deposited on the carbon film side and spread through the spin-coater.

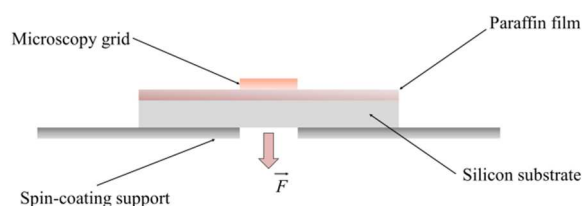


Figure 2 : Presentation of the setup used to deposit NPs on a carbon film grid using spin-coating method.

2.3. Instrumentation

2.3.1. High-angle annular dark-field scanning transmission electron microscopy (HAADF-STEM)

The TEM used in this study is the TEM JEOL 2200FS - 200 kV. The latter is equipped with a Schottky field emission gun operating at 200 kV. The microscope can be used for high-resolution imaging in TEM and STEM modes. Regarding STEM mode, the theoretical resolution that can be

achieved is estimated at 0.2 nm. This microscope is also equipped with an energy filter incorporated in the Omega-type column and a HAADF (High Angle Annular Dark Field) detector. This corresponds to an annular detector, coupled to a photomultiplier tube, which collects incoherently scattered electrons at very large angles. Here, HAADF-STEM was preferred to TEM for imaging nanoparticles with low atomic number because it is highly sensitive to the Z-contrast of the sample [35–38]. The parameters used for HAADF-STEM image acquisition are listed in Table 1.

Table 1 : parameters used for HAADF-STEM- image acquisition of silica NPs.

Parameter	Value
Voltage	200 kV
Probe current	10 pA
Magnification	x30 000
Resolution	8192 x 8192
Integration time per pixel	40 μ s
Semi-convergence beam	8 mrad
Camera length	40 cm
Semi-angle internal collection	78 mrad

Calibration of the transmission electron microscope is carried out using a grid supplied by the Ted Pella company and consisting in a bidirectional line array (Figure 3).

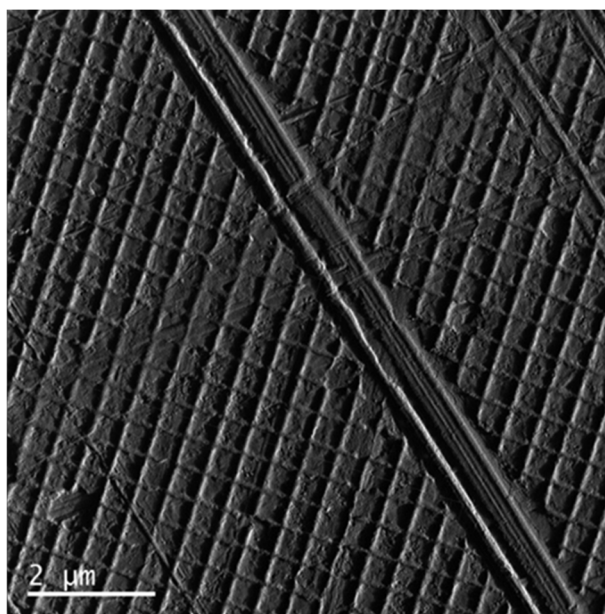


Figure 3 : HAADF-STEM image of Ted Pella 2160 lines/mm standard network.

The value given on this array is based on the number of lines per millimeter and is equal to 2160 lines/mm, i.e. an array pitch of 0.463 μm . From the STEM images of the array, the pixel size is estimated to be 1.156 nm.

2.3.2. Atomic force microscopy (AFM) in Peak Force[®] mode

The AFM images in Peak Force[®] mode were made on a Dimension Icon XR from Bruker. This instrument is equipped with a hybrid scanning system (Hybrid XYZ scanner head) allowing a displacement range of 90 μm x 90 μm x 14 μm respectively in the X, Y and Z directions with a closed-loop feedback control. The measurements were carried out using "Scan Assist-Air" tips. The AFM imaging parameters are listed in Table 2.

Table 2 : imaging parameters used for AFM Peak Force image acquisition of silica NPs deposited on carbon grid.

Imaging Parameter	Value
Image resolution	1024 x 1024
Scan size	5 μm x 5 μm
Scan rate	0.2 Hz
Amplitude	600 nm
Peak Force cycle frequency	0.5 kHz
Maximum applied force	400 pN

The AFM Z calibration is performed using structure TGZ01 from MikroMasch (Tallin, Estonia). It consists in a silicon calibration grating with a one dimensional array of rectangular steps with a step height of 18.5 ± 1.0 nm.

2.3.3. Scanning electron microscopy (SEM)

SEM images provided were performed with Field Emission Gun (FEG) SEM Zeiss Ultra Plus equipped with a GEMINI column. Images were acquired using an In-Lens secondary electron detector. From the manufacturer specifications, the electron beam size is roughly 1.7 nm at 1 kV accelerating voltage. Imaging and scanning parameters used in this study are listed in Table 3.

Table 3 : imaging and scanning parameters used for SEM image acquisition.

Scanning Parameter	Value
Accelerating voltage	3 kV
Working distance	3 mm
Magnification	40 kX
Image resolution	2048 x 1536
Pixel size	1.4 nm

Total imaging time

28.4 s

The image pixel size is controlled by measuring the pitch in X and Y directions of the reference structure P900H60 [25] using a Fourier transform.

3. Results and discussion

The novel approach described in this paper consists in using a single technique, HAADF-STEM to measure the dimensional characteristic parameters of a nanoparticle population in the three dimensions of space. However, the electron microscopy-based techniques provide no direct metrological information along the axis perpendicular to the scanning surface. In fact, data along Z -axis given in grey levels (GL) represent the intensity of the scattered electron signal. The experimental signal was fitted by a function regarding a sphere of D_{STEM} diameter and depending on two phenomenological parameters. As a first step, the signal linearity was checked and these parameters were determined using reference materials with a known thickness. The height, H_{SEM} , determined by this approach was also compared with the height measurements obtained by AFM considered as a reference technique. After testing the method on near-spherical nanoparticles, more complex shapes have been investigated.

3.1. Validation of the dimensional measurement technique by HAADF-STEM

3.1.1. HAADF-STEM signal linearity check using reference spherical particles (ERM®-FD101b)

In this section, we propose to analyze the intensity of the signal in order to determine the material thickness passed through by the electron beam. This is possible because the imaged particles in this work are chemically homogeneous. Thus, during STEM imaging, only the elastic scattering of electrons by the nuclei of the atoms influences the intensity of the collected signal. Assuming that the signal is linearly related to the thickness of the material crossed (on the thickness range studied), the signal I would be expressed by:

$$I = I_{sub} + \alpha h \quad (1)$$

With I_{sub} the intensity scattered by the substrate and h the thickness of the nanoparticle material under the electron beam. I_{sub} depends on the thickness of the carbon membrane, which may vary slightly, and on the dark signal from the HAADF detector. α is related to the imaging conditions and the material properties of the studied objects. In order to increase the display sensitivity, the dark signal of the HAADF detector, close to 30 000 GL (grey levels) is subtracted beforehand.

Since the thickness h of a spherical particle with diameter D can be described as a function of the x and y coordinates by :

$$h(x, y) = D \cdot \sin \left(\arccos \left(\frac{\sqrt{(x - x_0)^2 + (y - y_0)^2}}{\frac{D}{2}} \right) \right) \quad (2)$$

The expected HAADF signal generated when scanning a perfectly spherical nanoparticle should be equal to :

$$I(x, y, I_{sub}, \alpha, D, x_0, y_0) = I_{sub} + \alpha \cdot \left(D \cdot \sin \left(\arccos \left(\frac{\sqrt{(x - x_0)^2 + (y - y_0)^2}}{\frac{D}{2}} \right) \right) \right) \quad (3)$$

With x_0 and y_0 the positions of the centre of the sphere in the x and y directions.

To relate the HAADF-STEM signal intensity (expressed in grey level) to the thickness of the material passed through by the electron beam, ERM[®]-FD101b reference silica particles were used. Thus, it is possible to use the larger population of ERM[®]-FD101b suspension to check the linearity of the HAADF-STEM signal. In this way, I_{sub} and α calibration parameters for each image can be determined. The method used can be divided into the following steps:

- First, to locate the position of the different particles on the HAADF-STEM image, a threshold was set. The determination of the centroid positions in the x and y directions then enable the creation of thumbnails for each particle, which will be then processed independently.
- Then, each created thumbnail of individual spherical particle was fitted with equation (3) to check the linearity of the signal with the thickness passed through by electrons. Figure 4 presents the experimental signal (green) across a reference spherical particle, and the fit according to the function (3) (red). The residual image (subtraction of the adjustment from STEM signal) allows verifying the linearity hypothesis of the HAADF-STEM signal with the thickness of the nanoparticle (spherical) passed through by electrons (Figure 4).

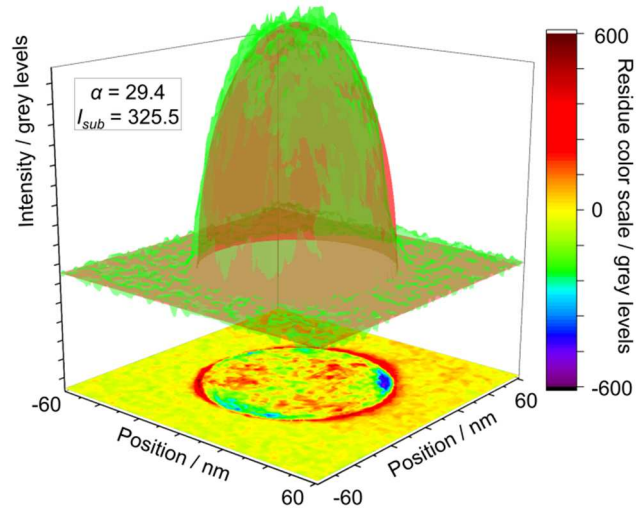


Figure 4 : HAADF-STEM signal of a reference silica particle ERM[®]-FD101b (green) and adjustment by the function (3) according to the x and y positions (red). The color scale bar (in GL) is associated to the difference between the HAADF-STEM signal and the adjustment (residual).

Overall, the residual image shows that equation (3) fits well the experimental signal, except on the particle contour, where a slight discrepancy is observed. This phenomenon is most probably related to the convolution between the Gaussian electron beam, having a size (standard deviation) of less than one nanometer, and the particle.

The method consisting in adjusting the function describing the thickness of material crossed in a sphere on the spherical HAADF-STEM signal is thus validated for this first particle. This shows that the intensity of the measured signal varies linearly with the crossed thickness passed through. This analysis has then been performed on all the particles extracted from the image to evaluate the I_{sub} and α parameters (about 100 particles on average per image).

Therefore, an $I(h)$ calibration function is available for all sample points on the condition that I_{sub} and α are determined for each new STEM image.

3.1.2. I_{sub} and α distribution analysis

The values of these two parameters was evaluated on different HAADF-STEM images of the silica suspension reference ERM[®]-FD101b. To follow the recommendations of the calibration certificate, only particles with a diameter greater than 60 nm are processed. A total of 400 ERM[®]-FD101b particles, divided over 4 images, were measured to determine the I_{sub} and α calibration parameters. The distributions of α and I_{sub} parameters, evaluated here for one HAADF-STEM image (138 thumbnails) are presented in Figure 5-a and Figure 5-b, respectively.

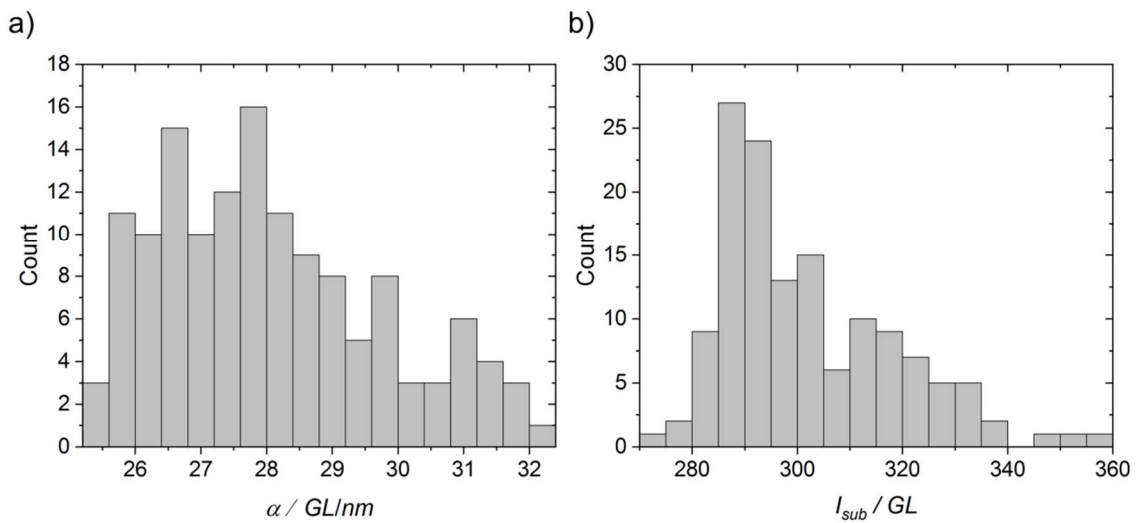


Figure 5 : Distributions of parameters a) α in GL (grey levels) per nm and b) I_{sub} in GL evaluated on the 138 extracted ERM[®]-FD101b thumbnails on one image.

For example on a first image, a mean value of 29.2 GL/nm was found for α with a standard deviation of 1.8 GL/nm for all the 138 particles of the image. This study was reproduced on 3 additional HAADF-STEM images, results are presented in Table 4.

Table 4 : mean α and I_{sub} values evaluated on 4 HAADF-STEM images.

Image	Number of NPs measured	α (GL/nm)	I_{sub} (GL)
1	138	29.2 ± 1.8	311.0 ± 17.6
2	63	28.5 ± 1.9	314.0 ± 19.1
3	75	31.0 ± 1.2	318.7 ± 16.7
4	124	28.1 ± 1.5	303.0 ± 19.2

For the first image, the scattering of the α values can be explained by the deviation from the sphericity of the silica particles studied. Indeed, an aspect ratio (height/diameter) equal to (0.95 ± 0.03) was found during a previous study for these particles [25]. In addition, noise in the HAADF-STEM image can also cause this dispersion. Regarding I_{sub} parameter, a mean value of 311.0 GL was obtained with a standard deviation of 17.6 GL for all 138 thumbnail of the image. In the next sections, the α and I_{sub} values will be fixed and equal to the mean values determined from all the particles on each image.

3.1.3. Evaluation of dimensional parameters H_{STEM} and D_{STEM} on the same set of silica nanoparticles

The I_{sub} and α calibration parameters are then used to calculate H_{STEM} , the maximum particle height determined from the STEM signal:

$$H_{STEM} = \frac{I_{max} - I_{sub}}{\alpha} \quad (4)$$

With I_{max} , the maximum signal intensity measured on the particle.

H_{STEM} results were then compared for each particle with the equivalent particle diameter measured by HAADF-STEM D_{STEM} . The D_{STEM} measurement is based on a binary image obtained by thresholding the signal at the base of the particle. In HAADF-STEM images, the ideal threshold to be applied is I_{sub} . However, in order to ignore noise and substrate roughness, the threshold is deliberately placed at a distance $3\sigma_{sub}$ from I_{sub} (σ_{sub} being the noise-related standard deviation of the signal corresponding to the substrate). The corresponding diameter is called $D_{measured}$. This offset causes a bias in the measurement of the equivalent projected surface diameter of the particle as shown in Figure 6.

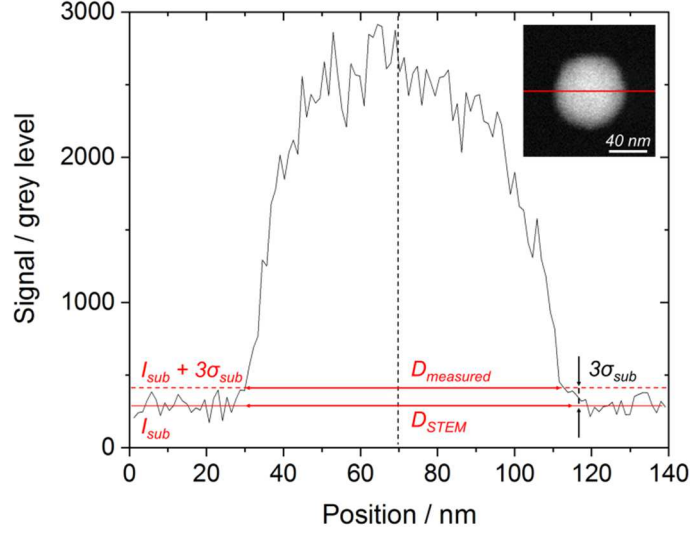


Figure 6 : Cross-sectional greyscale intensity profile of an ERM®-FD101b particle extracted along a scan line on a HAADF-STEM image.

It is then necessary to determine the bias between $D_{measured}$, the equivalent projected area diameter of the particle obtained after thresholding at an $I_{sub} + 3\sigma_{sub}$ position, and D_{STEM} , the particle diameter at the I_{sub} position. For this, the Taylor expansion of the arccos $\left(\frac{x-x_0}{\frac{D_{STEM}}{2}}\right)$ function when x tends towards $x_0 + D_{STEM}/2$ (at the edge of the particle) was carried out and gives :

$$\lim_{x \rightarrow x_0 + \frac{D_{STEM}}{2}} I(x) \sim I_{sub} + \alpha \cdot D_{STEM} \cdot \sqrt{2} \sqrt{1 - \left(\frac{x-x_0}{\frac{D_{STEM}}{2}}\right)} \quad (5)$$

At the threshold level one has :

$$\begin{cases} I = I_{sub} + 3\sigma_{sub} \\ x - x_0 = \frac{D_{measured}}{2} \end{cases} \quad (6)$$

Developing equation (5) from the conditions described in equation (6) gives the relationship between D_{STEM} and $D_{measured}$:

$$D_{STEM} = \frac{D_{measured} + \sqrt{D_{measured}^2 + \frac{18\sigma_{sub}^2}{\alpha^2}}}{2} \quad (7)$$

The comparison of H_{STEM} and D_{STEM} was then carried out on the particles extracted in the previous section (400 NPs). Results are shown in Figure 7.

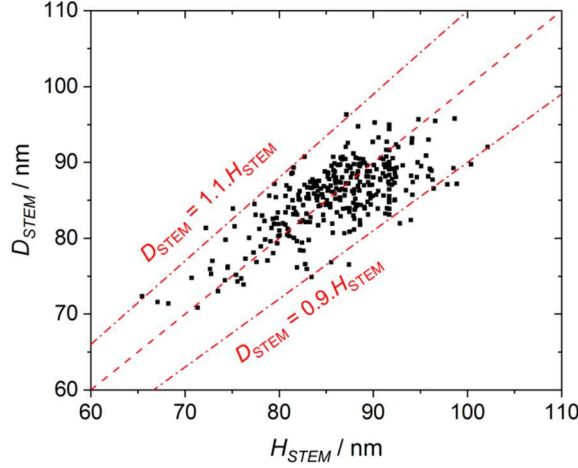


Figure 7 : Particle-by-particle comparison of D_{STEM} and H_{STEM} . The red dashed curve corresponds to the line $y = x$. The red dot-dash curves represent $D_{STEM} = 0.9.H_{STEM}$ and $D_{STEM} = 1.1.H_{STEM}$.

Results show that the D_{STEM} and H_{STEM} measurements are close to the $y = x$ curve. The mean aspect ratio H_{STEM}/D_{STEM} , for a total of 400 NPs is equal to (1.01 ± 0.05) . In addition, all results are within the range $[D_{STEM} = 0.9.H_{STEM}; D_{STEM} = 1.1.H_{STEM}]$. Compared to results obtained on the same nanoparticles in ref. [25] by AFM/SEM comparison ($H_{AFM}/D_{SEM} = 1.01 \pm 0.02$), a higher dispersion of measurements is observed. The latter can be attributed to the measurement uncertainties associated with H_{STEM} and D_{STEM} .

Indeed the uncertainty on H_{STEM} , $u(H_{STEM})$ is evaluated from equation (4) and is equal to [39] :

$$u(H_{STEM}) = \sqrt{\left(\frac{\partial H_{STEM}}{\partial I_{sub}}\right)^2 u^2(I_{sub}) + \left(\frac{\partial H_{STEM}}{\partial I_{max}}\right)^2 u^2(I_{max}) + \left(\frac{\partial H_{STEM}}{\partial \alpha}\right)^2 u^2(\alpha)} \quad (10)$$

With $u(I_{sub})$, $u(I_{max})$ and $u(\alpha)$, the uncertainties associated with the parameters I_{sub} , I_{max} and α , respectively.

For each measurement, $u(I_{sub})$ and $u(\alpha)$ correspond to the standard deviation associated with the I_{sub} and α parameters evaluated on spherical particles as shown in Figure 5. $u(I_{max})$ was associated with noise in HAADF-STEM images.

The uncertainty associated with D_{STEM} measurements was estimated from equation (9) and is equal to :

$$u(D_{STEM}) = \sqrt{\left(\frac{\partial D_{STEM}}{\partial D_{measured}}\right)^2 u^2(D_{measured}) + \left(\frac{\partial D_{STEM}}{\partial \sigma_{sub}}\right)^2 u^2(\sigma_{sub}) + \left(\frac{\partial D_{STEM}}{\partial \alpha}\right)^2 u^2(\alpha)} \quad (11)$$

With $u(D_{measured})$ and $u(\sigma_{sub})$, the uncertainties associated with $D_{measured}$ and σ_{sub} , respectively. $u(D_{measured})$ is linked to the uncertainty associated to the microscope calibration. Indeed, the uncertainty linked to the measurement depends only on the calibration.

Thus, as an example, regarding the ERM[®]-FD101b silica NP presented in Figure 6, H_{STEM} and D_{STEM} are equal to (80.9 ± 3.9) nm ($k = 1$) and (80.1 ± 0.9) nm ($k = 1$), respectively.

3.1.4. Comparison of dimensional parameter measurements using AFM, SEM and HAADF-STEM on a same set of nanoparticles

To validate the quantitative HAADF-STEM approach, D_{STEM} and H_{STEM} measurements performed on the ERM[®]-FD101b reference particles were compared to the measurements obtained by AFM and SEM on the same set of particles.

For this purpose, AFM and SEM images were performed on the particles constituting the larger mode of the ERM[®]-FD101b reference suspension observed previously by HAADF-STEM. The measurement method described in ref [40] was applied to determine the height of the particles by AFM. For SEM images, the segmentation method described in ref [41] was used. Detailed uncertainty budgets were carried out for the measurement of NPs using both techniques. Thus, they will be considered as reference techniques for this study. The AFM images were performed first to prevent the effects of specimen contamination from affecting the height measurement as described in ref [42]. A marker in the center of the microscopy grid enables to locate the area imaged by AFM and to find it easily by electron microscopy afterwards. Figure 8 a-c shows an example of the same area imaged by AFM, SEM and HAADF-STEM. A total of 45 particles were imaged and measured by AFM and HAADF-STEM, 191 NPs by SEM and HAADF-STEM. The comparison between H_{AFM} , *i.e.* the height measured by AFM, and H_{STEM} is presented in Figure 8-d. The same comparison was performed between D_{SEM} , *i.e.* the equivalent diameter measured by SEM, and D_{STEM} and is presented in Figure 8-e.

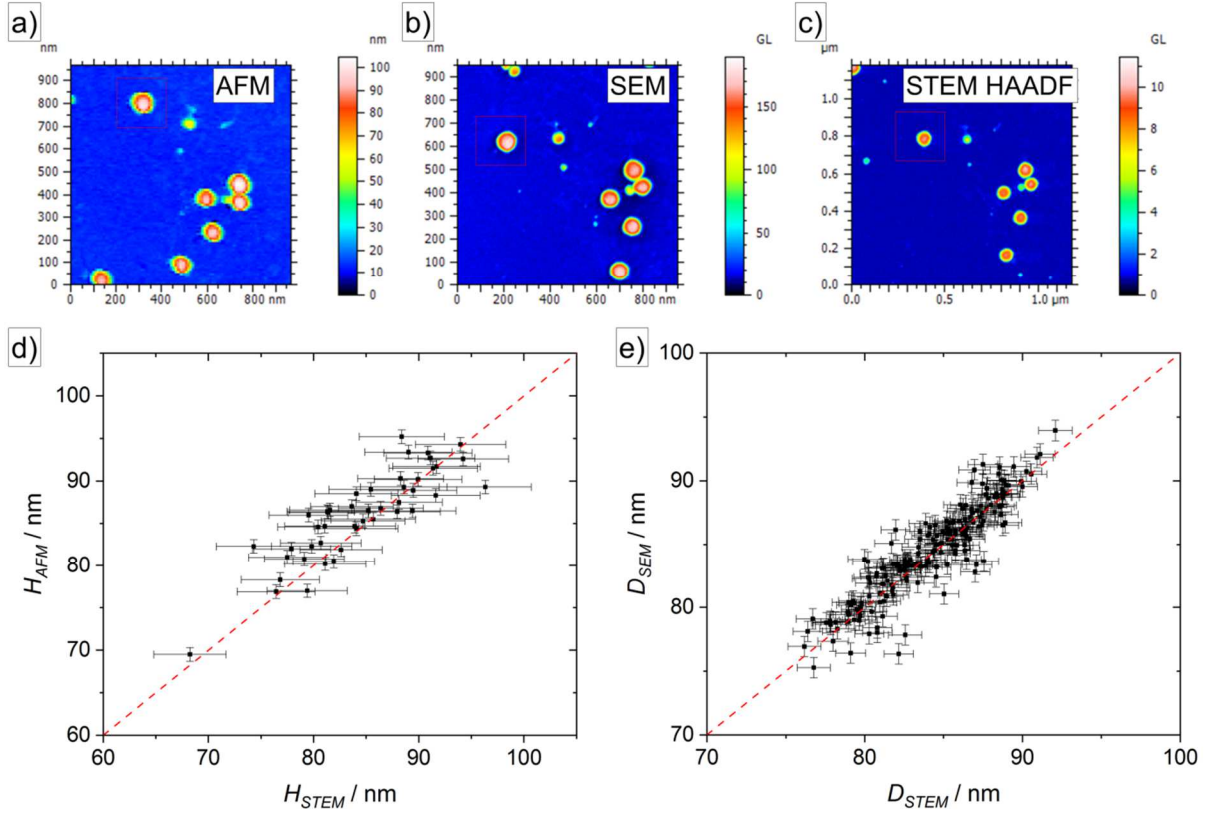


Figure 8 : Images a) AFM Peak Force, b) SEM and c) HAADF-STEM of the same area of a reference silica sample ERM®-FD101b deposited on carbon film. d) Particle-by-particle comparison of H_{STEM} and H_{AFM} . e) Particle-by-particle comparison of D_{STEM} and D_{SEM} . The red dashed curves correspond to the line $y = x$.

Thus, the height and diameter measurements performed by STEM are in good agreement, regarding measurement uncertainty, with those obtained by AFM and SEM ($k = 1$). Indeed, all the results are close to the $y = x$ curve. Therefore, with this comparison, one can validate the three-dimensional HAADF-STEM approach on silica particles. It is thus possible to determine the two calibration parameters α and I_{sub} directly on spherical particles present in the HAADF-STEM images. Uncertainties associated with H_{STEM} and D_{STEM} must be discussed. In both cases, a main contribution to the measurement uncertainty is related, directly or indirectly, to the noise in the HAADF-STEM image. Indeed, for $u(H_{STEM})$, the noise on the STEM signal contributes directly to $u(I_{max})$ and indirectly to $u(I_{sub})$ and $u(\alpha)$. Regarding $u(D_{STEM})$, $u(\sigma_{sub})$ and $u(\alpha)$ are linked to the noise. The reduction of noise in the image by applying for example a longer integration time per pixel could drastically reduce the measurement uncertainty.

3.2. Application on non-spherical particles

The HAADF-STEM approach has been validated using reference particles of well-known size and shape. In this section, we will use the HAADF-STEM method to analyze the morphology and dimensions of unknown nanoparticles with more complex shape.

In order to calculate α and I_{sub} , it is necessary to have a reference point on the images. Thus, there are two possible options to access this reference point. The approach applied and detailed in the continuation of this work for each case is as follows:

- The first case corresponds to a bi-population of nanoparticles, consisting of large spherical particles, which will serve as a calibration standard for the determination of the parameters α and I_{sub} , and smaller ellipsoidal particles, corresponding to the particles to be studied.
- The second case corresponds to a population consisting solely of ellipsoidal nanoparticles to be analyzed. In this case, without reference spherical particles, a measurement of the height of the individual particles will first be carried out by AFM. After identification of the same particles by STEM, this profile will be considered as input data to calibrate the parameters α and I_{sub} .

3.2.1. Bimodal population including spherical and non-spherical particles

As already mentioned, as I_{sub} and α depend on acquisition parameters that can vary from one image to another, they must be calculated for each HAADF-STEM image. In the previous section, the constituent particles of the second mode of the reference suspension ERM[®]-FD101b were used to determine these parameters by fitting the function (3) on the HAADF-STEM signal. However, this reference suspension has a small population whose constituent particles are more complex in shape with equivalent diameter close to 40.0 nm [31]. Here, the calibration parameters (I_{sub} and α) were evaluated on the 80.0 nm spherical NPs mode. Since the small particles constituting the first mode of the ERM[®]-FD101b reference suspension are present on the same STEM images, these parameters can then be used. Moreover, D_{STEM} was also determined for each particle as presented in section 3.3. The comparison of the individual measurements of H_{STEM} and D_{STEM} for a total of 917 NPs is presented in Figure 9.

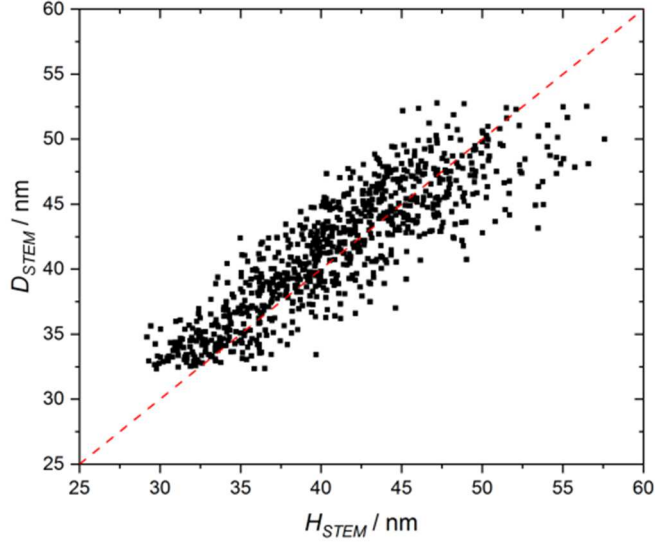


Figure 9 : Particle-by-particle comparison of D_{STEM} and H_{STEM} for the small population of reference silica particles ERM[®]-FD101b. The red dashed curve corresponds to the line $y = x$. All measurements are performed using calibration parameters α and I_{sub} determined on the large particles on the same image.

Results show a homogeneous distribution of the points around the line $y = x$. The mean aspect ratio (H_{STEM}/D_{STEM}) calculated on 917 NPs is equal to (0.99 ± 0.07) , 0.07 being the standard deviation on the aspect ratio of the particles. The results are in agreement with those obtained during the AFM/SEM comparison on identical particles (same suspension used) for which the (H_{AFM}/D_{SEM}) aspect ratio was equal to (0.95 ± 0.02) [25]. Here, the scattering in the measurement must be compared with the measurement uncertainty. Indeed, the uncertainty associated with H_{STEM} , $u(H_{STEM})$, evaluated as presented in section 3.3, is close to 3.0 nm ($k=1$), which represents 8% of the measured value.

Through this approach it is also possible to achieve a finer three-dimensional characterization of each particle. Indeed, knowing the calibration parameters (I_{sub} and α), one can fit equation (3) on the HAADF-STEM signal on each individual particle. This adjustment makes it possible to highlight the deviation from the sphericity of these small NPs as shown in Figure 10-a-d.

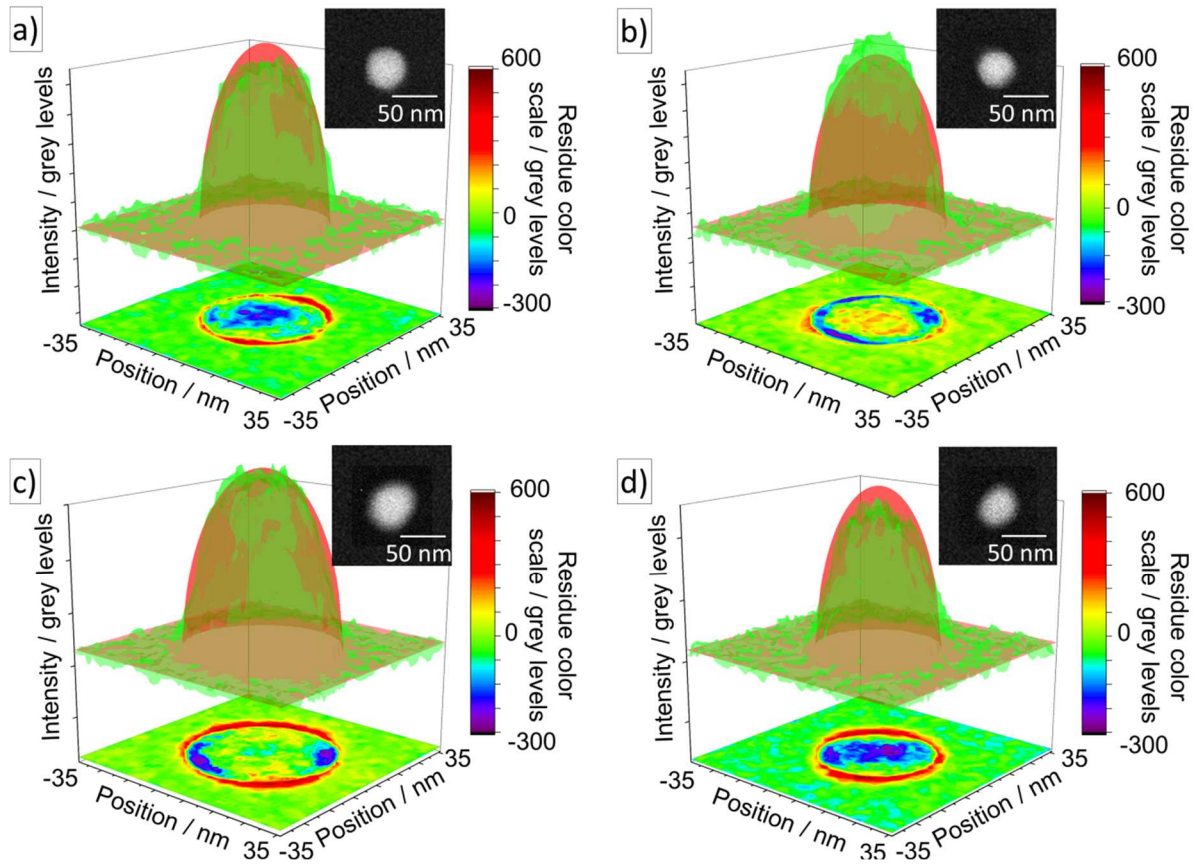


Figure 10 : (a-d) HAADF-STEM signal of four silica particles constituting the small population of reference suspension ERM[®]-FD101b (green) and adjustment by the function (3) according to the x and y positions with α and I_{sub} fixed (red). The color scale bar (in GL) is associated to the difference between the HAADF-STEM signal and the adjustment (residual).

Residual analysis corresponds to the difference between signal HAADF-STEM and adjustment by function (3). The results are shown in Figure 10 (graph included below HAADF-STEM signal) and this analysis allows a better understanding of the shape and orientation of the particles on the substrate. Each color spot matches deviation from sphericity of the nanoparticles.

- Figure 10-a: a significant discrepancy appears on the top and the contour of the particle in a uniform manner. The nanoparticle is a spheroid and the shape is clearly oblate
- Figure 10-b: On the edge, the adjustment is above the signal, whereas the opposite is true on the top. The nanoparticle is also a spheroid but the shape is prolate with a main axis perpendicular to the substrate surface.
- Figure 10-c: the residual signal consists of two red spot on two opposite sides of the edge and two blue spot on two other opposite sides. This configuration demonstrates the presence of three different axes (ellipsoid) and indicates the orientation of the nanoparticle with a major and minor axis parallel to the substrate surface.

- Figure 10-d: The shape is similar to the one shown in Figure 10-c, the particle is an ellipsoid. However, the large blue spot crossing the residue figure proves that the ellipsoidal nanoparticle is oriented in such a way that the major axis is parallel to the substrate and the minor axis is perpendicular to the substrate.

Consequently, this approach makes it possible to measure the particle length, width and height (assuming a regular spheroid/ellipsoid shape). This technique is therefore fast, notably in comparison with electron tomography techniques, which require a large number of images [43–45]. Other method, based on SEM and structure-from-motion photogrammetry, can also be used to perform accurate NP 3D characterization, but the challenges remain the same and specific substrate development is required [26]. Finally, the use of a single technique avoids the problems of sample transfer and co-location inherent to hybrid metrology [25]. But in this case, HAADF-STEM signal calibration was performed by imaging, in a same picture, particles of interest and particles of ideal shape (in our study spherical shape) with the same chemical composition.

3.2.2. Use of AFM measurements as reference point

In this section, the focus is now on the particles ERM®-FD304 (indicative diameter given at (27.8 ± 1.5) nm ($k = 2$) by the certificate), which have an ellipsoidal shape with three axes of different sizes. Contrary to the previous experiment, there is no reference particle in this sample to adjust the α and I_{sub} parameters. One solution would have been to add reference particles in the colloidal solution before deposition. Here, we use instead the complementarity between AFM and HAADF-STEM. Figure 11 presents the same particle observed both by AFM and HAADF-STEM.

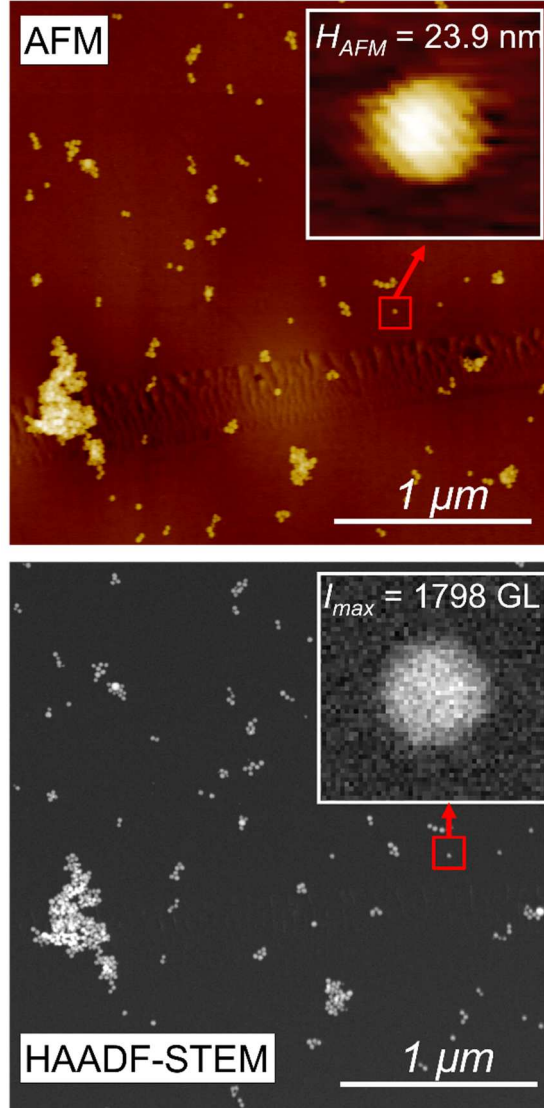


Figure 11 : AFM Peak Force and HAADF-STEM images of the same area of a reference silica sample ERM®-FD304 deposited on carbon film. The inserted images zoom in on the particle used to calibrate the HAADF-STEM signal from AFM Peak Force measurement.

Its height measured by AFM is equal to 23.9 nm. The maximum signal measured by HAADF-STEM on this particle is equal to 1798 GL. Knowing the I_{sub} parameter (average signal at the substrate level), the α parameter regarding equation (4) is equal to :

$$\alpha = \frac{I_{max} - I_{sub}}{h_{AFM}} \quad (12)$$

To achieve a better estimate of the α parameter, this approach was applied for at least 10 particles in each image. Then from the values of the calibration parameters α and I_{sub} , the H_{STEM} height measurements were performed on all the particles present on the image. D_{STEM} measurements were also performed on the same particles using the method describes in section 3.3. The comparison between H_{STEM} and D_{STEM} on the same NPs, for a total of 279 nano-objects, is presented in Figure 12.

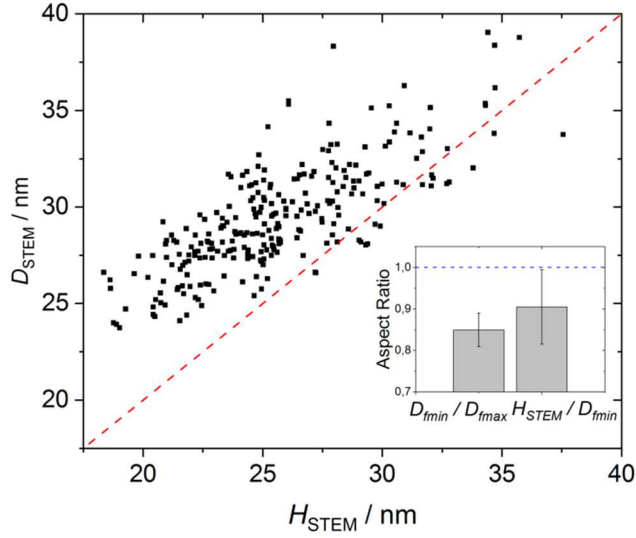


Figure 12 : Particle-by-particle comparison of D_{STEM} and H_{STEM} for the reference silica particles ERM[®]-FD304. The red dashed curve corresponds to the line $y = x$. The inserted figure represents the mean aspect ratio (D_{fmin}/D_{fmax}) and (H_{STEM}/D_{fmin}) calculated on the 279 NPs.

A systematic discrepancy is observed between H_{STEM} and D_{STEM} measurements with diameter larger. The same observation was performed in an hybrid AFM/SEM approach in ref. [25]. Feret diameter measurements (D_{fmin} = minimum Feret diameter and D_{fmax} = maximum Feret diameter) were also carried out on the particles to evaluate the deviations from the sphericity of the particles in the XY plane. The average aspect ratios of the 279 NPs in the three spatial dimensions (D_{fmin}/D_{fmax} and H_{STEM}/D_{fmin}) were evaluated. The results are presented in the insert of Figure 12. The mean aspect ratios (D_{fmin}/D_{fmax}) and (H_{STEM}/D_{fmin}) are respectively equal to (0.85 ± 0.04) and (0.90 ± 0.09) . These results are consistent with those of the AFM/SEM hybrid approach carried out on the same suspension [25]. Thus, the reference silica particles ERM[®]-FD304 have three axes of different sizes and are systematically deposited so that their major axis is parallel to the surface of the substrate.

Comparison of the HAADF-STEM signal with the adjustment by equation (3) with the parameters α and I_{sub} fixed makes it possible to confirm these observations. Moreover, thanks to the lateral resolution and the high sensitivity in grey level of HAADF-STEM, it is possible to go beyond the study of characteristic dimensions and perform a real study of the 3D morphology of nanoparticles. Two examples are shown in Figure 13-a and Figure 13-b.

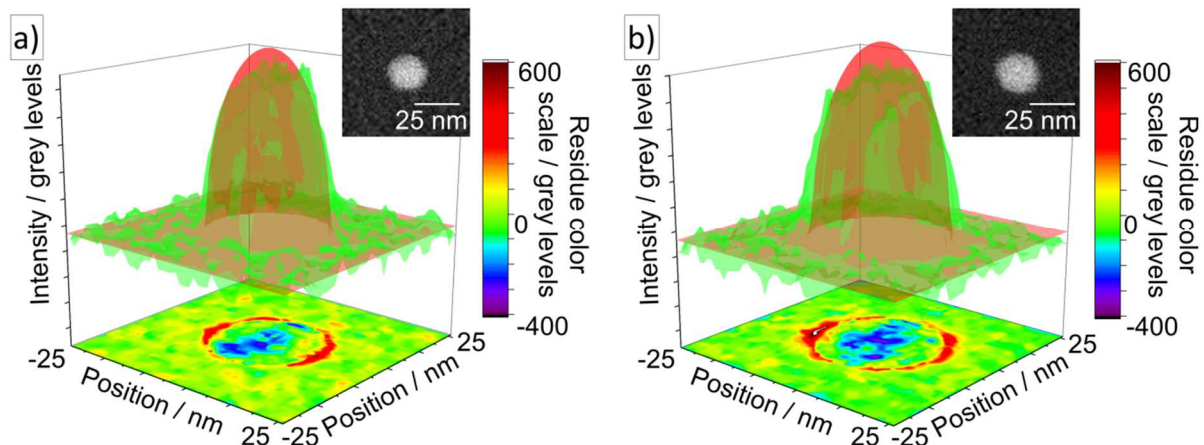


Figure 13 : (a-b) HAADF-STEM signal of reference silica particles ERM[®]-FD304 (green) and adjustment by the function (3) according to the x and y positions with a and I_{sub} fixed (red). The color scale bar (in GL) is associated to the difference between the HAADF-STEM signal and the adjustment (residual).

Thus, the analysis of the residues (difference between STEM signal and fit) confirms the hypothesis that the particles are ellipsoidal in shape with three axes of different dimensions. Indeed, in the XY plane, two differently sized and orthogonal axes are visible. Moreover, a symmetry of the shape of the particle is observable along these two axes. Finally, a deviation between fit and HAADF-STEM signal (represented in blue) is visible in the centre of the particle. This highlights a non-sphericity of the particles along this axis. Finally, in both cases, we observe that the deposited particles are oriented with their major axis parallel to the substrate. These results are consistent with ones obtained in the previous section.

4. Conclusions

An innovative method was developed to characterize the morphology of NPs in the three dimensions of space with a single instrument: the transmission electron microscope in HAADF-STEM mode.

This last technique offers the advantage, unlike SEM, of presenting a signal that can be directly related to the thickness of the material passed through by electrons when studying amorphous particles. The method consists in adjusting the HAADF-STEM signal by a function describing the thickness of material regarding a sphere of D_{STEM} diameter. The method was calibrated using reference material and the linearity of the HAADF-STEM signal with the thickness of the sample crossed by electron beam. The measured heights were compared with measurements carried out by AFM.

The three-dimensional analysis of these particles, carried out using a single instrument and a single image, allowed us to confirm the observations and results previously obtained with a hybrid approach combining AFM and SEM on the same nanoparticle population and propose a new finer and user-friendly approach of three dimensional analysis at nanoscale.

The 3D-characterization of more complex shape silica particles can also be carried out with this technique. For this, a reference is required on the images. This reference can be either a particle of known shape (with a similar chemical composition) or a particle whose height has been previously measured with another technique (AFM for instance). Thus, the study of the silica particles ERM[®]-FD304 by HAADF-STEM highlighted their spheroidal shape but also their preferential orientation on the substrate.

For example, regarding the regulation in force, this method will make it possible to measure the nanoscale dimension of nanoplates naturally oriented according to the sides with the larger surface area in contact with the substrate.

References

1. Weir A, Westerhoff P, Fabricius L, Hristovski K, von Goetz N (2012) Titanium Dioxide Nanoparticles in Food and Personal Care Products. *Environ Sci Technol* 46:2242–2250 . <https://doi.org/10.1021/es204168d>
2. Peters R, Dam G ten, Bouwmeester H, Helsper H, Allmaier G, Kammer F vd, Ramsch R, Solans C, Tomaniová M, Hajslova J, Weigel S (2011) Identification and characterization of organic nanoparticles in food. *TrAC Trends in Analytical Chemistry* 30:100–112 . <https://doi.org/10.1016/j.trac.2010.10.004>
3. He X, Hwang H-M (2016) Nanotechnology in food science: Functionality, applicability, and safety assessment. *Journal of Food and Drug Analysis* 24:671–681 . <https://doi.org/10.1016/j.jfda.2016.06.001>
4. Raj S, Jose S, Sumod US, Sabitha M (2012) Nanotechnology in cosmetics: Opportunities and challenges. *J Pharm Bioallied Sci* 4:186–193 . <https://doi.org/10.4103/0975-7406.99016>
5. Katz LM (2007) Nanotechnology and Applications in Cosmetics: General Overview. In: *Cosmetic Nanotechnology*. American Chemical Society, pp 193–200
6. Sbaji SJ, Boukhriss A, Majid S, Gmouh S (2020) Chapter 20 - The recent advances in nanotechnologies for textile functionalization. In: ul-Islam S, Butola BS (eds) *Advances in Functional and Protective Textiles*. Woodhead Publishing, pp 531–568
7. Wong YW, Yuen C, Leung MS, Ku S, Lam H (2006) SELECTED APPLICATIONS OF NANOTECHNOLOGY IN TEXTILES. *Autex Research Journal* 6:
8. Santos CSC, Gabriel B, Blanchy M, Menes O, García D, Blanco M, Arconada N, Neto V (2015) Industrial Applications of Nanoparticles – A Prospective Overview. *Materials Today: Proceedings* 2:456–465 . <https://doi.org/10.1016/j.matpr.2015.04.056>
9. Hainfeld JF, Powell RD (2000) New Frontiers in Gold Labeling. *J Histochem Cytochem* 48:471–480 . <https://doi.org/10.1177/002215540004800404>
10. Yezhelyev MV, Gao X, Xing Y, Al-Hajj A, Nie S, O'Regan RM (2006) Emerging use of nanoparticles in diagnosis and treatment of breast cancer. *The Lancet Oncology* 7:657–667 . [https://doi.org/10.1016/S1470-2045\(06\)70793-8](https://doi.org/10.1016/S1470-2045(06)70793-8)
11. Barbé C, Bartlett J, Kong L, Finnie K, Lin HQ, Larkin M, Calleja S, Bush A, Calleja G (2004) Silica Particles: A Novel Drug-Delivery System. *Advanced Materials* 16:1959–1966 . <https://doi.org/10.1002/adma.200400771>
12. Tang L, Cheng J (2013) Nonporous silica nanoparticles for nanomedicine application. *Nano Today* 8:290–312 . <https://doi.org/10.1016/j.nantod.2013.04.007>
13. Jeelani PG, Mulay P, Venkat R, Ramalingam C (2020) Multifaceted Application of Silica Nanoparticles. A Review. *Silicon* 12:1337–1354 . <https://doi.org/10.1007/s12633-019-00229-y>
14. Mathur P, Roy S (2020) Nanosilica facilitates silica uptake, growth and stress tolerance in plants. *Plant Physiology and Biochemistry* 157:114–127 . <https://doi.org/10.1016/j.plaphy.2020.10.011>

15. Jafari Daghlian Sofla S, James LA, Zhang Y (2018) Insight into the stability of hydrophilic silica nanoparticles in seawater for Enhanced oil recovery implications. *Fuel* 216:559–571 .
<https://doi.org/10.1016/j.fuel.2017.11.091>
16. Fakoya MF, Shah SN (2017) Emergence of nanotechnology in the oil and gas industry: Emphasis on the application of silica nanoparticles. *Petroleum* 3:391–405 .
<https://doi.org/10.1016/j.petlm.2017.03.001>
17. COMMISSION REGULATION (EU) 2018/1881 of 3 December 2018 amending Regulation (EC) No 1907/2006 of the European Parliament and of the Council on the Registration, Evaluation, Authorisation and Restriction of Chemicals (REACH) as regards Annexes I, III, VI, VII, VIII, IX, X, XI, and XII to address nanoforms of substances
18. Regulation (EU) 2015/2283 of the European Parliament and of the Council of 25 November 2015 on novel foods, amending Regulation (EU) No 1169/2011 of the European Parliament and of the Council and repealing Regulation (EC) No 258/97 of the European Parliament and of the Council and Commission Regulation (EC) No 1852/2001
19. Regulation (EU) No 528/2012 of the European Parliament and of the Council of 22 May 2012 concerning the making available on the market and use of biocidal products Text with EEA relevance
20. Regulation (EC) No 1223/2009 of the European Parliament and of the Council of 30 November 2009 on cosmetic products (Text with EEA relevance)
21. ISO/TR 13014 :2012, Guidance on physico-chemical characterization of engineered nanoscale materials for toxicologic assessment.
22. Lim J, Yeap SP, Che HX, Low SC (2013) Characterization of magnetic nanoparticle by dynamic light scattering. *Nanoscale Res Lett* 8:381–381 . <https://doi.org/10.1186/1556-276X-8-381>
23. Langevin D, Lozano O, Salvati A, Kestens V, Monopoli M, Raspaud E, Mariot S, Salonen A, Thomas S, Driessen M, Haase A, Nelissen I, Smisdom N, Pompa PP, Maiorano G, Puntès V, Puchowicz D, Stępnik M, Suárez G, Riediker M, Benetti F, Mičetić I, Venturini M, Kreyling WG, van der Zande M, Bouwmeester H, Milani S, Rädler JO, Mühlhopt S, Lynch I, Dawson K (2018) Inter-laboratory comparison of nanoparticle size measurements using dynamic light scattering and differential centrifugal sedimentation. *NanoImpact* 10:97–107 .
<https://doi.org/10.1016/j.impact.2017.12.004>
24. Laborda F, Jiménez-Lamana J, Bolea E, Castillo JR (2013) Critical considerations for the determination of nanoparticle number concentrations, size and number size distributions by single particle ICP-MS. *J Anal At Spectrom* 28:1220–1232 . <https://doi.org/10.1039/C3JA50100K>
25. Crouzier L, Delvallée A, Ducourtieux S, Devoille L, Noircler G, Ulysse C, Taché O, Barruet E, Tromas C, Feltin N (2019) Development of a new hybrid approach combining AFM and SEM for the nanoparticle dimensional metrology. *Beilstein J Nanotechnol* 10:1523–1536 .
<https://doi.org/10.3762/bjnano.10.150>
26. Tondare VN (2020) A Concept for Three-Dimensional Particle Metrology Based on Scanning Electron Microscopy and Structure-from-Motion Photogrammetry. *Journal of Research of the National Institute of Standards and Technology* 125:NA

27. Buhr E, Bug MU, Bergmann D, Cizmar P, Frase CG (2017) Simultaneous measurement of lateral and vertical size of nanoparticles using transmission scanning electron microscopy (TSEM). *Measurement Science and Technology* 28:034002 . <https://doi.org/10.1088/1361-6501/28/3/034002>
28. Chen Z, Weyland M, Sang X, Xu W, Dycus JH, LeBeau JM, D'Alfonso AJ, Allen LJ, Findlay SD (2016) Quantitative atomic resolution elemental mapping via absolute-scale energy dispersive X-ray spectroscopy. *Ultramicroscopy* 168:7–16 . <https://doi.org/10.1016/j.ultramic.2016.05.008>
29. LeBeau JM, Findlay SD, Allen LJ, Stemmer S (2008) Quantitative Atomic Resolution Scanning Transmission Electron Microscopy. *Phys Rev Lett* 100:206101 . <https://doi.org/10.1103/PhysRevLett.100.206101>
30. Verleysen E, Bender H, Richard O, Schryvers D, Vandervorst W (2011) Compositional characterization of nickel silicides by HAADF-STEM imaging. *Journal of Materials Science* 46:2001–2008 . <https://doi.org/10.1007/s10853-010-5191-z>
31. Ramaye Y, Kestens V, Braun A, Linsinger TPJ, Held A, Roebben G (2017) The certification of equivalent diameters of silica nanoparticles in aqueous solution: ERM[®]-FD101b
32. Katrin F, Adelina B, Jean C-G, Olivier C, Vikram K, Andree LM, Thomas L, Gert R (2012) Certification of the equivalent spherical diameters of silica nanoparticles in aqueous solution - Certified Reference Material ERM[®]-FD304
33. Ogi T, Modesto-Lopez LB, Iskandar F, Okuyama K (2007) Fabrication of a large area monolayer of silica particles on a sapphire substrate by a spin coating method. *Colloids and Surfaces A: Physicochemical and Engineering Aspects* 297:71–78 . <https://doi.org/10.1016/j.colsurfa.2006.10.027>
34. Delvallée A, Feltn N, Ducourtieux S, Trabelsi M, Hochepped JF (2015) Direct comparison of AFM and SEM measurements on the same set of nanoparticles. *Measurement Science and Technology* 26:085601 . <https://doi.org/10.1088/0957-0233/26/8/085601>
35. Karlsson LS, Deppert K, Malm J-O (2006) Size Determination of Au Aerosol Nanoparticles by Off-Line TEM/STEM Observations. *Journal of Nanoparticle Research* 8:971–980 . <https://doi.org/10.1007/s11051-006-9094-5>
36. Pennycook SJ, Chisholm MF, Lupini AR, Varela M, Borisevich AY, Oxley MP, Luo WD, van Benthem K, Oh S-H, Sales DL, Molina SI, García-Barriocanal J, Leon C, Santamaría J, Rashkeev SN, Pantelides ST (2009) Aberration-corrected scanning transmission electron microscopy: from atomic imaging and analysis to solving energy problems. *Philosophical Transactions of the Royal Society A: Mathematical, Physical and Engineering Sciences* 367:3709–3733 . <https://doi.org/10.1098/rsta.2009.0112>
37. Zhang B, Zhang W, Su DS (2011) Towards a More Accurate Particle Size Distribution of Supported Catalyst by using HAADF-STEM. *ChemCatChem* 3:965–968 . <https://doi.org/10.1002/cctc.201100096>
38. Dippong T, Levei EA, Cadar O (2017) Preparation of CoFe₂O₄/SiO₂ Nanocomposites at Low Temperatures Using Short Chain Diols. *Journal of Chemistry* 2017:7943164 . <https://doi.org/10.1155/2017/7943164>

39. International Organization for Standardization (2008) ISO/IEC Guide 98-3, Uncertainty of measurements – Part 3 : Guide to the expression of uncertainty in measurements
40. Delvallée A, Feltin N, Ducourtieux S, Trabelsi M, Hochepped JF (2015) Toward an uncertainty budget for measuring nanoparticles by AFM. *Metrologia* 53:41–50 . <https://doi.org/10.1088/0026-1394/53/1/41>
41. Crouzier L, Delvallée A, Ducourtieux S, Devoille L, Tromas C, Feltin N (2019) A new method for measuring nanoparticle diameter from a set of SEM images using a remarkable point. *Ultramicroscopy* 207:112847 . <https://doi.org/10.1016/j.ultramic.2019.112847>
42. Crouzier L, Delvallée A, Allard A, Devoille L, Ducourtieux S, Feltin N (2019) Methodology to evaluate the uncertainty associated with nanoparticle dimensional measurements by SEM. *Measurement Science and Technology* 30:085004 . <https://doi.org/10.1088/1361-6501/ab1495>
43. Saghi Z, Holland DJ, Leary R, Falqui A, Bertoni G, Sederman AJ, Gladden LF, Midgley PA (2011) Three-Dimensional Morphology of Iron Oxide Nanoparticles with Reactive Concave Surfaces. A Compressed Sensing-Electron Tomography (CS-ET) Approach. *Nano Lett* 11:4666–4673 . <https://doi.org/10.1021/nl202253a>
44. Thomas JM, Midgley PA, Ducati C, Leary RK (2013) Nanoscale electron tomography and atomic scale high-resolution electron microscopy of nanoparticles and nanoclusters: A short surveyNanoscale electron tomography and atomic scale high-resolution electron microscopy of nanoparticles and nanoclusters: A short surveyretain-->. *Progress in Natural Science: Materials International* 23:222–234 . <https://doi.org/10.1016/j.pnsc.2013.04.003>
45. Altantzis T, Zanaga D, Bals S (2017) Advanced electron tomography of nanoparticle assemblies. *EPL (Europhysics Letters)* 119:38001 . <https://doi.org/10.1209/0295-5075/119/38001>